Nonlinear Temperature Gradient Effect on Maximum Warping Stresses in Rigid Pavements

BOUZID CHOUBANE AND MANG TIA

The results are presented of an experimental and analytical study to determine the actual temperature distribution within typical concrete pavement slabs and to evaluate the effects of nonlinear thermal gradients on the behavior of concrete pavements. The temperature data obtained in this study indicated that the temperature variations within the pavement slabs were mostly nonlinear. The temperature distribution throughout the depth of a concrete pavement slab can be represented fairly well by a quadratic equation. When the distribution is nonlinear, the maximum computed tensile stresses in the slab tend to be lower for the daytime condition and higher for the nighttime condition as compared with the stresses computed with the consideration of a linear temperature distribution.

Daily temperature fluctuation within the concrete slab is an important factor affecting concrete pavement behavior. Thermally induced slab movements could significantly influence (a) the load transfer between adjacent slabs and (b) the degree of support offered by the subgrade, which affect the maximum load-induced stresses in the concrete slab. Several methods for rigid pavement design and analysis that take into account the effect of these temperature fluctuations have been developed over the years. These methods are all based, for simplicity, on the assumption that the temperature variation in the concrete slab from top to bottom is linear, even though the nonlinearity of the temperature distribution throughout the slab has long been recognized.

The nonlinearity of temperature distribution within the concrete pavement slab was first measured in the Arlington Road tests in the early 1930s. Teller and Sutherland, the investigators, concluded then that a uniform temperature gradient would result in the most critical stress condition, even though the curved gradient was the more usual temperature distribution (*1*). In 1940 Thomlinson reached the same conclusion by assuming a simple harmonic temperature variation at the slab top surface in combination with the heat flow laws (*2*). The magnitudes of the stresses derived in both cases were compared with those given by Westergaard's equations. Bradbury used a temperature differential in the concrete slab in his warping stress equations in plain and reinforced concrete pavements (*3*). According to Lang (*4*), the variations of the temperature distribution from the straight-line relationship are relatively small. The maximum measured temperature difference between a straight line and the actual distribution was less than 2°F at 2.5 and 4.5 in. below the slab surface for a 7-in. slab thickness. Lang concluded that considering the importance of the warping stress and the many variables affecting the design, these small variations from a straight line are not important, and consequently the temperature gradient can be approximated as linear for convenience.

With the advent of the computer age, various finite-element computer models that allow considerable freedom in loading configuration, flexural stiffness, and boundary conditions have been developed. Most of the currently used computer programs, such as WESLIQID (*5*), WESLAYER (*5*), JSLAB (*6*), ILLI-SLAB (*7*), and FEACONS (*8,9*), consider only the linear temperature gradient effects on the concrete slab.

In this paper the results are presented of an experimental and analytical study to determine the actual temperature distribution within typical concrete pavement slabs and to evaluate the effect of a nonlinear thermal gradient on the behavior of concrete pavements.

SLAB INSTRUMENTATION AND DATA COLLECTION

A six-slab concrete pavement constructed at the Materials Office of the Florida Department of Transportation (FDOT) was used to monitor pavement temperatures for this investigation. Each slab is 20 ft long, 12 ft wide, and 9 in. thick. The adjoining Slabs 1 and 2 and Slabs 4 and 5 are connected by dowels, as shown in Figure 1.

The test pavement was constructed to be representative of in-service Florida concrete pavements in August 1982. The slabs were laid on a native roadbed soil consisting mainly of granular materials classified as A-3 according to the AASHTO Soil Classification. The average limerock bearing ratio (LBR) of the compacted subgrade was 50 (*9*).

Five thermocouples to monitor pavement temperatures were embedded in the slab concrete at different levels at the time of construction. These thermocouples are positioned at 1, 2.5, 4.5, 6.5 and 8 in. below the top surface at the center of the fourth slab. The ambient temperature was measured by another thermocouple that was housed inside a wooden box mounted on a 5-ft pole. The thermocouples were connected to a Fluke programmable data logger. For the purpose of this study, the data logger was programmed to take the temperature measurements from all five sensors at 15-min intervals.

Department of Civil Engineering, University of Florida, Gainesville, Fla. 32611.

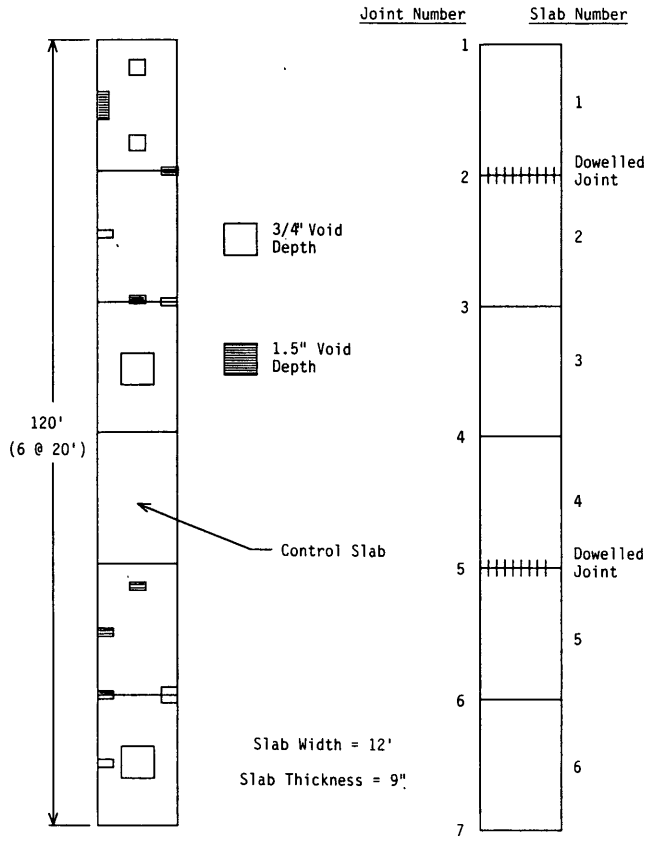

FIGURE 1 Plan of test slabs.

THERMAL GRADIENT ANALYSIS

Recorded Temperature Distribution

Figures 2 through 5 show the typical recorded variations in temperature distribution throughout the test slab for various times of the day at different periods of the year. It can be seen that the temperature differential in the slab tends to be positive in the daytime and negative at night. The nonlinearity of the temperature distribution is apparent. In addition, the curvature of the temperature distribution tends to be inward when ΔT is positive and outward when ΔT is negative. The temperature distributions for the nighttime and daytime conditions, which are used in the thermal stress analyses in this study, are based on the characteristics of these typical recorded temperature data.

Typical Thermal Gradient Components

The temperature distribution in the pavement slab can be typically divided into three components: (a) a component that causes axial displacement, that is, overall expansion or contraction; (b) a component that causes the bending; and (c) the nonlinear component, as shown in Figure 6.

The division of the temperature distribution into these three components is based on the assumption used in classical plate-bending theory that the cross section of a plate remains plane after bending. Thus, the plate can deform in only two ways:

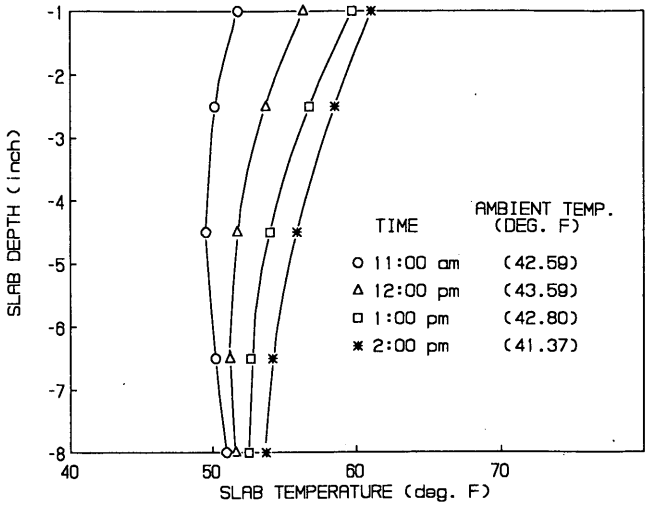

FIGURE 2 Typical daily temperature variations throughout the test slab corresponding to a positive temperature differential as recorded in January.

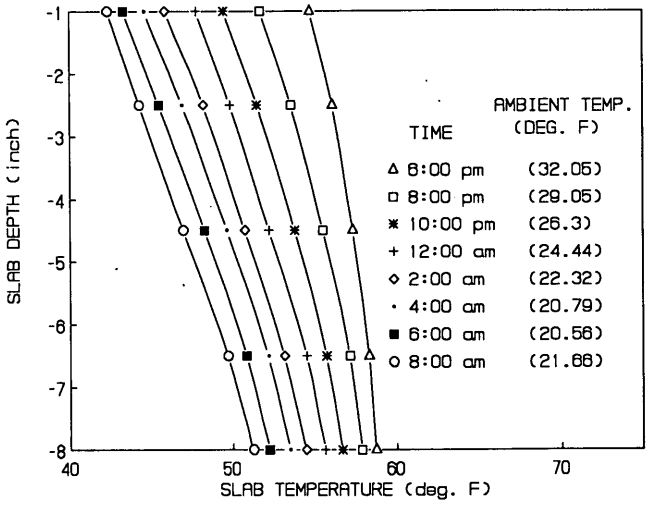

FIGURE 3 Typical daily temperature variations throughout the test slab corresponding to a negative temperature differential as recorded in January.

it can expand or contract axially, or it can bend with its cross section remaining plane. The first type of deformation is caused by a uniform temperature component. The second type is caused by a linear temperature distribution. The nonlinear temperature component is the remaining temperature component after the uniform and the linear temperature components have been subtracted from the total temperature distribution. These three temperature components are shown in Figure 6(a–c).

Mathematical Modeling of the Thermal Gradient

In order to isolate and study the effect of the nonlinearity of temperature variation, a mathematical model was used. From

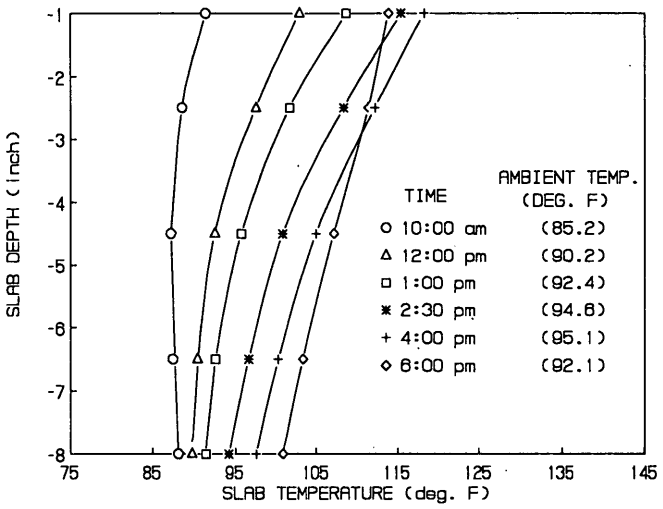

FIGURE 4 Typical daily temperature variations throughout the test slab corresponding to a positive temperature differential as recorded in July.

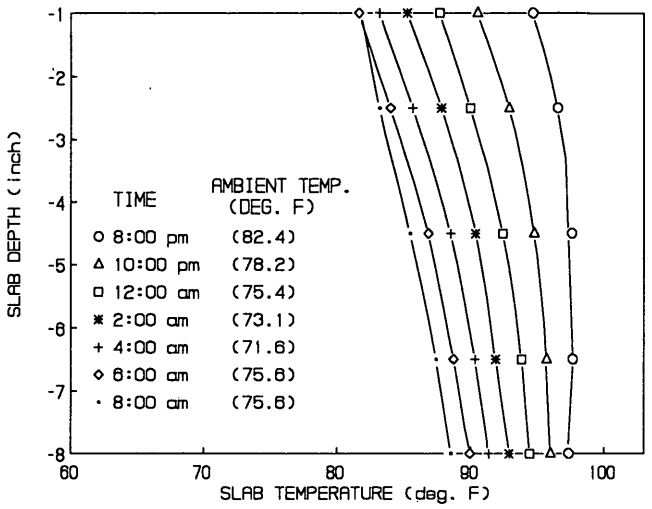

FIGURE 5 Typical daily temperature variations throughout the test slab corresponding to a negative temperature differential as recorded in July.

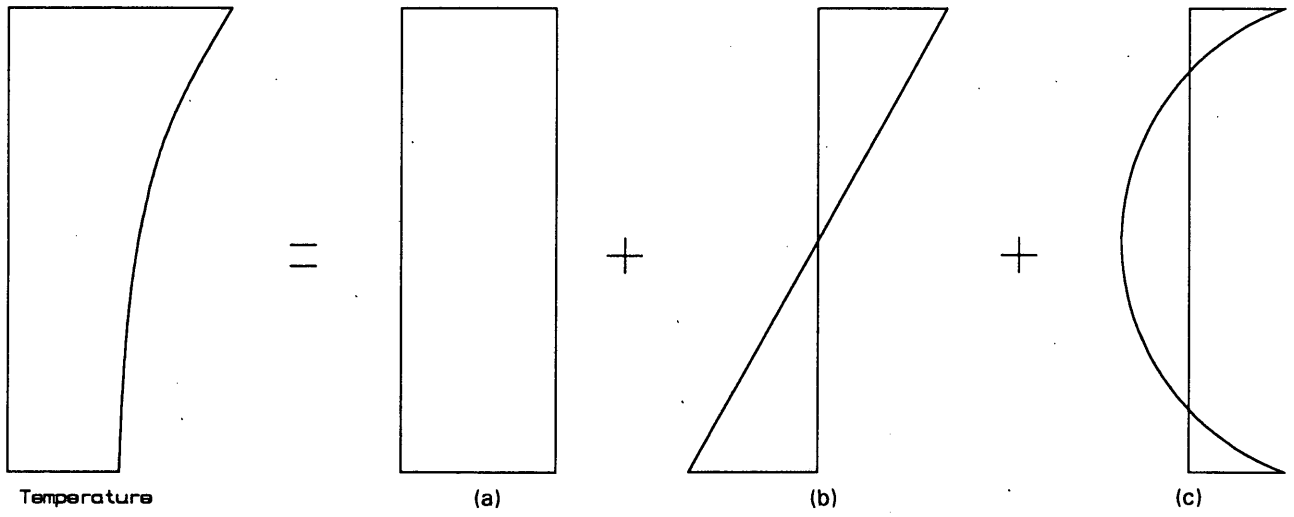

FIGURE 6 Typical temperature variation profile throughout a slab and its three components: (a) component causing axial displacement, (b) component causing bending, and (c) nonlinear temperature component.

an analysis of the temperature data and comparative study of the existing models for predicting actual temperature distributions, it appeared that a quadratic equation could be used to express the temperature as a function of depth. This is shown in Figures 7 and 8. The general form of the equation is

$$t = A + By + Cy^2 \tag{1}$$

where t is the temperature in degrees Fahrenheit and y is the slab depth, with $y = 0$ at the top and $y = d$ at the bottom.

Since a quadratic equation can be defined by three points, the quadratic equation is determined by matching the equation with the measured temperatures at three points. If these three temperature readings were taken at the top (t_t), at the middle (t_m), and at the bottom of the slab (t_b), the coefficients A, B, and C would be defined as follows:

$$A = t_t \tag{2}$$

$$B = (4t_m - 3t_t - t_b)/d \tag{3}$$

$$C = 2(t_t + t_b - 2t_m)/d^2 \tag{4}$$

Table 1 summarizes the representative values of these coefficients A, B, and C as well as the corresponding temperature differentials for a daily cycle at various time periods.

The temperature component causing axial displacement is determined by integrating the temperature across the section and dividing the integral (area under the curve) by the slab thickness as follows:

$$t_{\text{axial}} = \frac{1}{d}\int_0^d (A + By + Cy^2)dy$$

$$= A + B(d/2) + C(d^2/3) \tag{5}$$

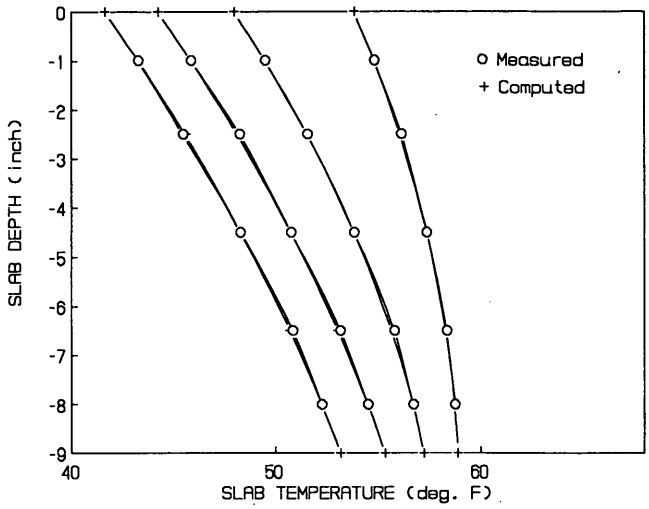

FIGURE 7 Computed versus measured temperature variations throughout the test slab corresponding to a negative temperature differential as recorded in a typical daily cycle in January.

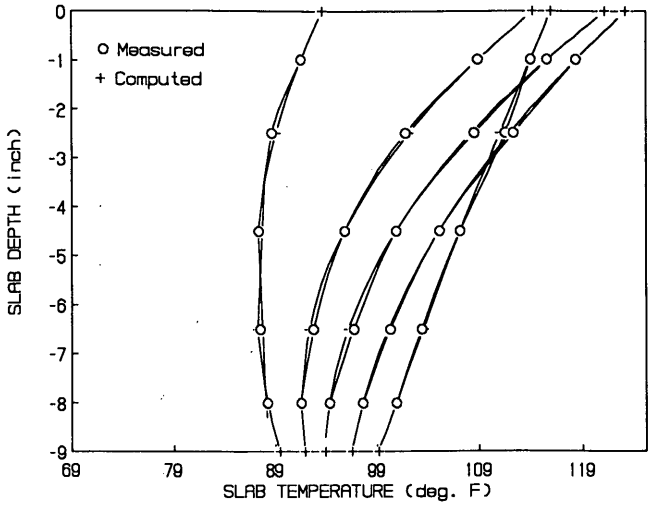

FIGURE 8 Computed versus measured temperature variations throughout the test slab corresponding to a positive temperature differential as recorded in a typical daily cycle in January.

TABLE 1 Representative Values of the Coefficients *A*, *B*, and *C* of Quadratic Equation 1 as Computed for a Daily Cycle at Various Time Periods

Period of the Year	Typical Daily Cycle Time	A	B	C	Temp. Diff. DT
Jan.	11:00 am	53.03836	-1.45816	0.149795	0.99
	01:00 pm	62.11836	-2.58102	0.172653	9.24
	02:00 pm	63.05142	-2.13142	0.12	9.46
	06:00 pm	53.80979	1.010408	-0.05020	- 5.03
	08:00 pm	50.41081	1.408367	-0.05918	- 7.88
	10:00 pm	47.97265	1.578979	-0.06163	- 9.22
	00:00 am	46.37285	1.477142	-0.04	-10.05
	02:00 am	44.24959	1.669387	-0.04897	-11.06
	04:00 am	42.90612	1.734897	-0.05102	-11.48
	06:00 am	41.67204	1.671632	-0.04367	-11.51
June	09:00 am	98.73816	-3.31775	0.239591	10.45
	11:00 am	112.3161	-4.91938	0.263265	22.95
	01:00 pm	122.8802	-5.95183	0.281632	30.75
	03:00 pm	109.18	-0.35714	-0.14285	14.78
	05:00 pm	115.2114	-2.54857	0.057142	18.31
	08:00 pm	96.50530	1.727959	-0.18326	- 0.71
	10:00 pm	91.15979	1.796122	-0.13591	- 5.16
	00:00 am	87.80530	1.662244	-0.09755	- 7.06
	02:00 am	85.18428	1.605714	-0.08	- 7.97
	06:00 am	82.31448	1.246734	-0.04122	- 7.88
Nov.	10:00 pm	59.27816	2.189387	-0.11755	-10.18
	02:00 am	54.90693	2.133265	-0.09020	-11.89
	04:00 am	53.41183	2.090612	-0.08244	-12.14
	07:00 am	51.39204	2.085918	-0.07795	-12.46
	10:00 am	68.82632	-2.87265	0.256326	5.09
	12:00 pm	82.05326	-4.76653	0.323265	16.71
	01:18 pm	87.53387	-4.97346	0.299591	20.49
	04:00 pm	74.87102	0.336530	-0.09755	4.87

The temperature component causing bending of the slab is determined by taking the moment of the area that remains after the axial component is subtracted from the total area under the curve and then finding a linear temperature distribution that would produce the same moment.

The moment is taken with respect to the mid-depth of the slab. Let $y' = (d/2) - y$
Then

$$t_{total} - t_{axial} = By + Cy^2 - B(d/2) - C(d^2/3)$$
$$= -C(d^2/12) - (B + Cd)y' + Cy'^2 \quad (6)$$

The moment, taken with respect to slab mid-depth, will then be as follows:

$$M = \int_{-d/2}^{d/2} (t_{total} - t_{axial})y'dy' = -(B + Cd)d^3/12 \quad (7)$$

For a linear temperature distribution varying from $+T_{curling}$ to $-T_{curling}$, the moment caused by this temperature distribution is

$$M = 2T_{curling}\,(d/4)\,(d/3) = T_{curling}\,(d^2/6) \quad (8)$$

By setting this moment equal to the moment as expressed in Equation 7, $t_{curling}$ at any depth y can be solved to be

$$t_{curling} = (B + Cd)\,[y - (d/2)] \quad (9)$$

Last, the nonlinear temperature component is determined as follows:

$$t_{nonlinear} = t_{total} - t_{axial} - t_{curling}$$
$$= C[y^2 - dy + (d^2/6)] \quad (10)$$

From this expression, it is apparent that if the coefficient C is positive, the extreme fibers of the slab would tend to expand. This condition is reversed if the coefficient C is negative. Furthermore, it can also be seen from Table 1 that this coefficient C, the nonlinear temperature component, is not directly correlated with the temperature differential.

In the case of the assumption of a linear temperature gradient, where the coefficient C is zero, only two temperature components would remain: the temperature component related to axial displacement and the curling temperature component related to slab bending.

Comparison with Other Models

Various models for predicting temperatures in concrete pavements have been developed by researchers such as Thomlinson (*2*), Barber (*11*), Bergstrom (*12*), Thompson et al. (*13*), and Hsieh et al. (*14*). Hsieh presented a three-dimensional computer model that uses the finite-difference scheme of Beam and Warming (*15*). The model is based on the coupled theories of heat-moisture conduction through a semifinite, isotropic, and homogeneous porous medium. The inputs required for this computer program are weather data and the material properties of the concrete and soil.

A comparison made between the computed temperature variations using Hsieh's computer model and the quadratic Equation 1 is shown in Figures 9 and 10. The predicted temperature variations from Hsieh's model match well with those from the quadratic equation unless there is a drastic change in temperature in the top 2 in. of the slab, as can be seen in Figure 9. In that case, if the temperature differential is positive, the quadratic equation gives comparatively higher temperatures in the top half of the slab and lower temperatures in the lower half. This observation is reversed in the case of a negative temperature differential.

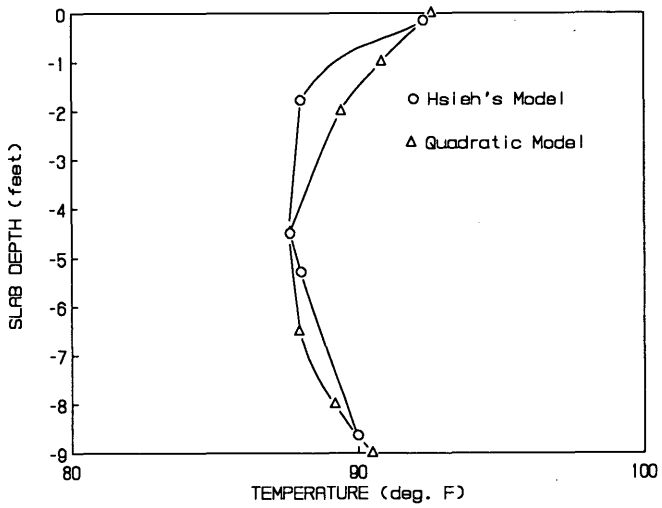

FIGURE 9 Predicted temperature distributions throughout the slab depth using the quadratic equation and Hsieh's model for full-sun simulation at 8:00 a.m.

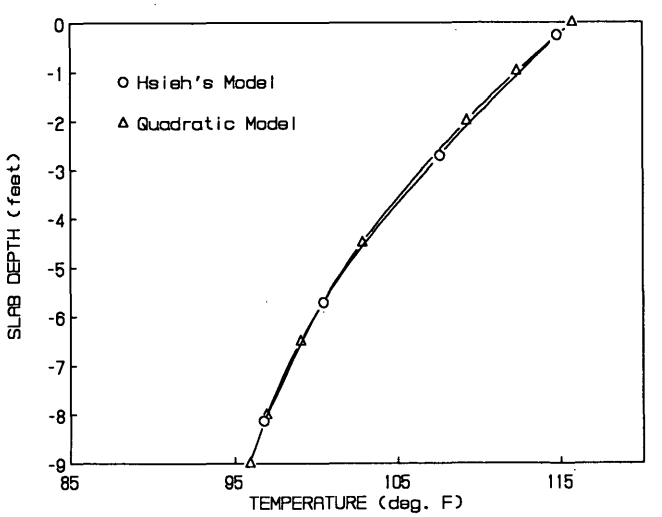

FIGURE 10 Predicted temperature distributions throughout the slab depth using the quadratic equation and Hsieh's model for full-sun simulation at 2:00 p.m.

THERMAL STRESS ANALYSIS

Bradbury's Equations for Computing Thermal Stresses

Several methods of determining thermal warping stresses were proposed as early as 1926 when Westergaard presented his well-known mathematical analysis on the subject. Using Westergaard's concepts, Bradbury (*3*) developed equations for the computation of the temperature-induced warping stresses at different positions of concrete pavement slabs.

The general Bradbury expressions for computing warping stresses due to temperature differential are as follows:

Edge stress:

$$\sigma = C_x E \alpha \Delta T/2 \tag{11}$$

Interior stresses:

$$\sigma_x = (E\alpha\Delta T/2)\,[(C_x + \mu C_y)/(1 - \mu^2)] \tag{12}$$

$$\sigma_y = (E\alpha\Delta T/2)\,[(C_y + \mu C_x)/(1 - \mu^2)] \tag{13}$$

where

E = modulus of elasticity of concrete,
α = thermal coefficient of expansion of concrete,
ΔT = temperature difference between top and bottom of the slab, and
C_x, C_y = warping stress coefficients.

The coefficients C_x and C_y are functions of the free length and width depending on the direction in which the curling stress is required. The values of these warping stress coefficients are given by Bradbury's nomograph (*3*).

FEACONS IV Computer Program

The computer program FEACONS IV (Finite Element Analysis of CONcrete Slabs, version IV) was developed at the University of Florida for analysis of the response of jointed concrete pavements to load and temperature variations (*8,9*). In this program, a jointed concrete pavement is modeled as a three-slab system, whereas a slab is considered as an assemblage of rectangular elements with three degrees of freedom per node as developed by Melosh (*16*) and Zienkiewicz and Cheung (*17*). The subgrade is assumed as a Winkler foundation modeled by a series of vertical springs at the nodes. Load transfers across the joints are modeled by linear and rotational springs connecting the slabs at the nodes of the elements along the joints. The thermal gradient across the depth of the slab is assumed to be uniform, and a temperature differential between the top and bottom surfaces of the slab is used as an input to the program.

Results from FEACONS Versus Bradbury's Equations

The thermal stresses caused by the temperature variation recorded from the test slabs were computed by using FEACONS and also by using Bradbury's equation for comparison purposes. For a slab 20 ft long, 12 ft wide, and 9 in. thick with an assumed coefficient of thermal expansion of 6×10^{-6}/°F, a modulus of elasticity of 4,500 ksi, a Poisson's ratio of 0.2 for the concrete, and a subgrade modulus of 300 pci, the coefficients C_x and C_y are determined to be equal to 1.064 and 0.609, respectively. Then Equations 11 through 13 become the following:

Edge stress:

$$\sigma = 14.364\Delta T \tag{14}$$

Interior stresses:

$$\sigma_x = 16.675\Delta T \tag{15}$$

$$\sigma_y = 11.556\Delta T \tag{16}$$

From the foregoing equations, it can be observed that the maximum computed warping stresses according to Bradbury's formulas occur at the interior of the slab and run in the longitudinal direction. Table 2 gives the typical values of computed thermal stresses according to Bradbury's equations along with the corresponding computed stresses from FEACONS. The computed stresses from Bradbury's equations are slightly higher than those from FEACONS for the daytime conditions, whereas they are very close to one another for the nighttime conditions. It is believed that the differences are due to the fact that FEACONS can take into account the possible loss of contact between the slab and the subgrade, although Bradbury's method does not.

Stress Analysis Considering Nonlinear Temperature Variation

Since the cross section of the slab is assumed to remain plane, the nonlinear temperature component, which does not cause any axial or bending deformation, will induce stresses in the slab as if the slab were totally restrained from deformation. The thermal stresses induced by the nonlinear temperature component as expressed in Equation 10 can be determined by multiplying the negative of the nonlinear temperature component by the coefficient of thermal expansion and the modulus of elasticity of concrete as follows:

$$\sigma = -E_c \alpha t_{\text{nonlinear}} = -E_c \alpha C[y^2 - dy + (d^2/6)] \tag{17}$$

This stress is a function of the coefficient C, the coefficient of thermal expansion, and the concrete modulus of elasticity. It can be seen that the variation of the coefficient of thermal expansion will affect the thermal stresses greatly.

Since the nonlinear temperature component does not affect the bending of the concrete slab, its effects on the total stresses in the concrete slab would be independent of the effects of the other factors. Thus, the total stress can be obtained by adding algebraically the bending stress due to a linear temperature gradient as computed by FEACONS and the corresponding stress due to the nonlinear component of the temperature distribution.

TABLE 2 Representative Values of Maximum Warping Stresses as Computed for a Daily Cycle Using Bradbury's Equations and FEACONS IV

Period of the Year	Typical Daily Cycle Time	Temperature Differential	Stresses (psi)	
			Bradbury	FEACONS IV
January	11:00 am	0.99	17	16
	1:00 pm	9.24	154	147
	2:00 pm	9.46	158	151
	6:00 pm	- 5.03	84	84
	8:00 pm	- 7.88	131	128
	10:00 pm	- 9.22	154	149
	00:00 am	-10.05	168	161
	2:00 am	-11.06	184	176
	4:00 am	-11.48	191	181
	6:00 am	-11.51	192	181
June	9:00 am	10.45	174	164
	11:00 am	22.95	383	310
	1:00 pm	30.75	513	418
	3:00 pm	14.78	246	228
	5:00 pm	18.31	305	263
	8:00 pm	- 0.71	12	12
	10:00 pm	- 5.16	86	86
	00:00 am	- 7.06	118	116
	2:00 am	- 7.97	133	129
	6:00 am	- 7.88	131	128
November	10:00 pm	-10.18	170	163
	2:00 am	-11.89	198	187
	4:00 am	-12.14	202	191
	7:00 am	-12.46	208	194
	10:00 am	5.09	85	84
	12:00 pm	16.71	279	249
	1:18 pm	20.49	342	295
	4:00 pm	4.87	81	80

The temperature data recorded on the test slabs were used to determine the thermal stresses in the concrete slabs by taking the effects of the nonlinear temperature component into account. The concrete was assumed to have a constant coefficient of thermal expansion of 6×10^{-6}/°F and a modulus of elasticity of 4,500 ksi. The stress due to the nonlinear temperature component in a 9-in. thick slab is given by the following expression:

$$\sigma = -27C(y^2 - 9y + 13.5) \quad (18)$$

From this expression, it can be seen that if coefficient C is positive, the extreme fibers of the slab would tend to expand and cause internal compressive stresses at these positions, and tensile stresses would result at slab mid-length. This condition is reversed if coefficient C is negative. This observation is valid for any slab thickness.

Representative values of stresses due to the nonlinear temperature component, bending stresses due to the linear temperature component, and the total stresses as determined in a daily cycle for various time periods are shown in Table 3. As a convention, the tensile stresses are computed as positive values and the compressive stresses are negative. It can be observed from Table 2 that the maximum compressive stresses due to the nonlinear temperature component generally occurred between noon and 1:00 p.m.

Since concrete is much weaker in tension than in compression, the tensile stresses are much more critical than the compressive stresses and thus are of more concern. From Table 3 it can be observed that a nonlinear temperature distribution tends to increase the total maximum tensile stress in the slab at night when the temperature differentials are negative, whereas it tends to reduce the maximum tensile stress during the day when positive temperature differentials occur. A maximum stress of 240 psi due to the consideration of a nonlinear temperature distribution was computed for the condition at 6:00 a.m. during April, whereas the computed stress without the consideration of the nonlinear temperature effects was 216 psi. This amounts to an increase of approximately 11 percent in tensile stress. Conversely, a maximum computed bending stress of 418 psi was obtained for June at 1:00 p.m., whereas the corresponding computed total stress with the

TABLE 3 Representative Computed Total Stresses at the Extreme Slab Fibers Caused by Nonlinear Temperature Distribution in a Daily Cycle

Period of the Year	Typical Daily Cycle Time	STRESSES (psi)				
		Non-Linear	Bending		Total	
		Top & Bottom	Top	Bottom	Top	Bottom
January	11:00 am	-55	-16	16	-71	-39
	12:00 pm	-67	-102	102	-169	35
	01:00 pm	-63	-147	147	-210	84
	02:00 pm	-44	-151	151	-195	107
	06:00 pm	18	84	-84	102	-66
	10:00 pm	22	149	-149	171	-127
	02:00 am	18	176	-176	194	-158
	06:00 am	16	181	-181	197	-165
	08:00 am	6	56	-56	62	-51
April	10:00 am	-106	-154	154	-260	48
	12:00 pm	-116	-309	309	-425	193
	01:00 pm	-97	-352	352	-448	255
	02:00 pm	-79	-359	359	-438	280
	04:00 pm	0	-250	250	-250	250
	08:00 pm	58	112	-112	170	-54
	00:00 am	31	174	-174	205	-143
	04:00 am	27	200	-200	227	-173
	06:00 am	24	216	-216	240	-192
June	11:00 am	-96	-310	310	-406	214
	01:00 pm	-103	-418	418	-521	315
	03:00 pm	52	-228	228	-176	280
	05:00 pm	-21	-263	263	-284	242
	08:00 pm	67	12	-12	79	55
	00:00 am	36	116	-116	152	-80
	06:00 am	15	128	-128	143	-113
July	08:00 pm	48	56	-56	104	-8
	00:00 am	40	139	-139	179	-99
	04:00 am	37	167	-167	204	-130
	06:00 am	31	170	-170	201	-139
	10:00 am	-76	-70	70	-146	-6
	12:00 pm	-116	-250	250	-366	134
	02:30 pm	-119	-371	371	-490	252
	04:00 pm	-85	-362	362	-447	277
	06:00 pm	-6	-249	249	-255	243
August	09:00 am	-19	50	-50	30	-69
	12:00 pm	-107	-258	258	-365	151
	03:16 pm	-116	-378	378	-494	262
	07:00 pm	68	-51	51	17	119
	08:00 pm	60	9	-9	69	51
	00:00 am	54	129	-129	183	-75
	04:00 am	36	145	-145	181	-109
	06:00 am	31	147	-147	178	-116

(*continued on next page*)

TABLE 3 (*continued*)

Period of the Year	Typical Daily Cycle Time	STRESSES (psi)				
		Non-Linear	Bending		Total	
		Top & Bottom	Top	Bottom	Top	Bottom
November	08:00 pm	48	140	-140	188	-92
	12:00 am	40	181	-181	221	-141
	04:00 am	30	191	-191	221	-161
	07:00 am	28	194	-194	222	-166
	10:00 am	-93	-84	84	-177	-9
	12:00 pm	-118	-249	249	-367	131
	01:18 pm	-109	-295	295	-404	186
	02:00 pm	83	-287	287	-370	204
	04:00 pm	36	-80	80	-44	116

consideration of the nonlinear temperature effects was 315 psi. This represents a 25 percent reduction in computed tensile stress. A maximum percent increase in computed tensile stress of 661 percent was obtained in August when the consideration of the effects of nonlinear temperature distribution increased the slab tensile stress from 9 to 69 psi.

SUMMARY OF FINDINGS

The main findings in this study are summarized as follows:

1. The temperature data obtained from the concrete test road in this study indicated that the temperature distribution within the concrete slabs is mostly nonlinear.
2. The temperature distribution throughout the depth of a concrete pavement slab can be represented fairly well by a quadratic equation.
3. When the temperature distribution is assumed to be linear, the maximum computed tensile stresses in the slab tend to be higher for the daytime condition and lower for the nighttime condition as compared with the stresses computed with the consideration of the effects of the nonlinear temperature distribution.

REFERENCES

1. L. W. Teller and E. C. Sutherland. The Structural Design of Concrete Pavements. *Public Roads*, Vol. 23, No. 8, June 1943, pp. 167–211.
2. J. Thomlinson. Temperature Variations and Consequent Stresses Produced by Daily and Seasonal Temperature Cycles in Concrete Slabs. *Concrete and Construction Engineering,* 1940.
3. R. D. Bradbury. *Reinforced Concrete Pavements.* Wire Reinforcement Institute, Washington, D.C., 1938.
4. F. C. Lang. Temperature and Moisture Variations in Concrete Pavements. *HRB Proc.*, Vol. 21, 1941, pp. 260–271.
5. Y. T. Chou. *Structural Analysis Computer Programs for Rigid Multicomponent Pavement Structures with Discontinuities—WESLIQID and WESLAYER.* Technical Reports 1, 2, and 3. U.S. Army Engineering Waterways Experiment Station, Vicksburg, Miss., May 1981.
6. S. P. Tayabji and B. E. Colley. *Analysis of Jointed Concrete Pavements.* FHWA, U.S. Department of Transportation, 1981.
7. A. M. Tabatabaie and E. J. Barenberg. Finite Element Analysis of Jointed or Cracked Concrete Pavements. In *Transportation Research Record 671*, TRB, National Research Council, Washington, D.C., 1978, pp. 11–19.
8. M. Tia, J. M. Armaghani, C. L. Wu, S. Lei, and K. L. Toye. FEACONS III Computer Program for an Analysis of Jointed Concrete Pavements. In *Transportation Research Record 1136*, TRB, National Research Council, Washington, D.C., 1987, pp. 12–22.
9. M. Tia, C. L. Wu, B. E. Ruth, D. Bloomquist, and B. Choubane. *Field Evaluation of Rigid Pavements for the Development of a Rigid Pavement Design System*—Phase III. Final Report, Project 245-D54. Department of Civil Engineering, University of Florida, Gainesville, July 1988.
10. J. M. Armaghani. *Comprehensive Analysis of Concrete Pavement Response to Temperature and Load Effects.* Ph.D dissertation. Department of Civil Engineering, University of Florida, Gainesville, 1987.
11. E. S. Barber. Calculation of Maximum Pavement Temperature from Weather Reports. In *Highway Research Board Bulletin 168,* HRB, National Research Council, Washington, D.C., 1975.
12. K. C. Bergstrom. Temperature Stresses in Concrete Pavements. Proc., Swedish Cement and Concrete Institute, Stockholm, 1950.
13. M. R. Thompson, B. Dempsey, H. Hill, and J. Vogel. Characterizing Temperature Effects for Pavement Analysis and Design. Presented at 66th Annual Meeting of the Transportation Research Board, Washington, D.C., 1987.
14. C. K. Hsieh, Q. Chaobin, and E. E. Ryder. *Development of Computer Modeling for Prediction of Temperature Distribution Inside Concrete Pavements.* Florida Department of Transportation, Department of Mechanical Engineering, University of Florida, Gainesville, Aug. 1989.
15. R. M. Beam and R. F. Warming. An Implicit Factored Scheme for the Compressible Navier-Stokes Equations. *AIAA Journal*, Vol. 16, No. 4, 1978, pp. 393–402.
16. R. M. Melosh. Basis of Derivation of Matrices for the Direct Stiffness Method. *AIAA Journal*, Vol. 1, No. 7, July 1963, pp. 1631–1637.
17. O. C. Zienkiewicz and Y. K. Cheung. The Finite Element Method for Analysis of Elastic Isotropic and Orthotropic Slabs. *Proc. Institute of Civil Engineers,* Vol. 28, 1964, pp. 471–488.